Acta Biomaterialia 144 (2022) 210–220

Contents lists available at ScienceDirect

Acta Biomaterialia

journal homepage: www.elsevier.com/locate/actbio

Full length article

On multiscale tension-compression asymmetry in skeletal muscle

Markus Böl[a,*], Stephan Kohn[a], Kay Leichsenring[a], Enrique Morales-Orcajo[a], Alexander E. Ehret[b,c]

[a] Institute of Mechanics and Adaptronics, Technische Universität Braunschweig, D-38106 Braunschweig, Germany
[b] Empa, Swiss Federal Laboratories for Materials Science and Technology, CH-8600 Dübendorf, Switzerland
[c] Institute for Mechanical Systems, ETH Zurich, CH-8092, Zürich, Switzerland

ARTICLE INFO

Article history:
Received 11 October 2021
Revised 11 March 2022
Accepted 17 March 2022
Available online 23 March 2022

Keywords:
Skeletal muscle
Porcine biceps femoris muscle
Tension-compression asymmetry
Passive experiments
Muscle tissue
Muscle fibre
Volume changes

ABSTRACT

Skeletal muscle tissue shows a clear asymmetry with regard to the passive stresses under tensile and compressive deformation, referred to as tension-compression asymmetry (TCA). The present study is the first one reporting on TCA at different length scales, associated with muscle tissue and muscle fibres, respectively. This allows for the first time the comparison of TCA between the tissue and one of its individual components, and thus to identify the length scale at which this phenomenon originates. Not only the passive stress-stretch characteristics were recorded, but also the volume changes during the axial tension and compression experiments. The study reveals clear differences in the characteristics of TCA between fibres and tissue. At tissue level TCA increases non-linearly with increasing deformation and the ratio of tensile to compressive stresses at the same magnitude of strain reaches a value of approximately 130 at 13.5% deformation. At fibre level instead it initially drops to a value of 6 and then rises again to a TCA of 14. At a deformation of 13.5%, the tensile stress is about 6 times higher. Thus, TCA is about 22 times more expressed at tissue than fibre scale. Moreover, the analysis of volume changes revealed little compressibility at tissue scale whereas at fibre level, especially under compressive stress, the volume decreases significantly. The data collected in this study suggests that the extracellular matrix has a distinct role in amplifying the TCA, and leads to more incompressible tissue behaviour.

Statement of significance

This article analyses and compares for the first time the tension-compression asymmetry (TCA) displayed by skeletal muscle at tissue and fibre scale. In addition, the volume changes of tissue and fibre specimens with application of passive tensile and compressive loads are studied. The study identifies a key role of the extracellular matrix in establishing the mechanical response of skeletal muscle tissue: It contributes significantly to the passive stress, it is responsible for the major part of tissue-scale TCA and, most probably, prevents/balances the volume changes of muscle fibres during deformation. These new results thus shed light on the origin of TCA and provide new information to be used in microstructure-based approaches to model and simulate skeletal muscle tissue.

1. Introduction

With a mass fractions of around 40% for the average human [1] and up to 60% for athletes [2], the skeletal musculature constitutes a substantial part of the human body and forms the basic component of the musculoskeletal system that allows motion. It serves as a shock absorber, protects the skeleton from external overload, and plays a major role in body metabolism. In recent years, muscle function and muscle mechanics have also increasingly been investigated in medical and socio-economic aspects, such as disease [e.g. 3–5] or ageing [e.g. 6,7].

Recent experimental studies have dealt with the passive mechanical characterisation of muscle tissue, in which mostly strips or cube-shaped tissue samples prepared from muscles are tested.

* Corresponding author.
E-mail address: m.boel@tu-braunschweig.de (M. Böl).

https://doi.org/10.1016/j.actbio.2022.03.034

Beside the realisation of pure shear compression experiments [8,9], tissue samples were mostly subjected to axial tension [10–16] and axial compression [17–25] experiments. In addition to the observation that the behaviour is non-linear, strongly anisotropic, and viscoelastic, a notable feature, which can be also found in other biological tissues [26–30], is the so-called tension-compression asymmetry (TCA).

In case of skeletal muscle tissue Takaza et al. [31] and Mohammadkhah et al. [32] reported that the passive tensile stress-stretch response is two orders of magnitude larger than in passive compression, which indicates a significant TCA. From a mechanical point of view, TCA may be considered as a phenomenon caused by different load transfer mechanisms for tension and compression within the tissue while the material properties of the tissue's constituents remain the same. Consequently, it seems evident that the pronounced TCA of muscle tissue is directly related to its microstructure. Following Listrat et al. [33], muscle tissue contains 75% water, 20% protein, 1–10% fat, and 1% glycogen. Thereby the tissue is strongly structured at different levels of organisation: Visible with the naked eye, muscle tissue consists of muscle fibre bundles embedded into connective tissue, the extracellular matrix (ECM). The ECM in turn, is structured into three sub-layers. The endomysium is located around the single muscle fibres, the perimysium groups muscle fibres to fascicles, and the epimysium surrounds the entire muscle. For more details, especially with respect to the impact of ECM on load transfer mechanisms, the reader is referred to Böl et al. [8] and Kohn et al. [34].

Although TCA in muscle tissue is a non-negligible mechanical phenomenon, dedicated studies are rare. Microstructural investigations by Takaza et al. [31] on porcine muscle tissue revealed a significant change of fibre shape with applied tensile and compressive loads on the tissue specimen. The authors hypothesised that parts of the ECM (endomysium and perimysium) are responsible for the TCA. Further investigations of the same group [35] described the three-dimensional structure of collagen in the perimysium for porcine and chicken skeletal muscle and revealed that in the undeformed situation the perimysium sheets show a waviness that increases or decreases, depending on the applied external deformation. However, the source of TCA could be not explained.

While the aforementioned studies have mainly focused on the ECM to understand the phenomenon of TCA, little is known on TCA at fibre level and corresponding detailed studies are largely missing. While the majority of studies deal with tension experiments on muscle fibre bundles [36–43], muscle fibres [36,38,39,42,44–54], myofibrils [55–58], and proteins [57,59,60], axial compression experiments on the muscle fibre scale have only been reported twice by our own group [61,62], to the best of the authors' knowledge. In Böl et al. [61] TCA at fibre scale was reported for the first time, observing an approximately ten-fold stiffer stress-stretch behaviour under tension compared to compression loading.

Towards understanding the source of TCA, but also towards completing the understanding of muscle tissue function, the analysis of tissue and fibre level volume changes during deformation is of great interest. While at the tissue level such information is partly available in the form of measured Poisson's ratios, ranging between 0.34 and 0.64 for compressive and from 0.17 to 0.83 for tensile loading (measured by means of markers attached to the tissue sample) in dependence on the fibre orientation and species [15,22,32], and three-dimensional imaging based volume measurements [17,8], such information is still extremely rare at fibre level, and appears to be limited to the study by Smith et al. [63] who report only insignificant volume reductions under tensile loading for isolated muscle fibres but up to 60% volume loss for fibre bundles, calculated from images, respectively.

Consequently, the aim of this paper is to analyse, compare, and evaluate the relationship between the microscopic (fibre level) and macroscopic (tissue level) response in terms of passive mechanical stress-stretch relations and deformation-dependent volume changes at both levels in order to draw conclusions on the origin of TCA observed at tissue level. We will refer to these levels as 'length-scales' in the sense of a multiscale study noting that a change of scale does not only imply different dimensions but also a change from the homogenised tissue response to the fibre as a single component. It is expected that this study will lead to an improved understanding of the phenomenon of TCA and that it will serve as a basis to develop, inform, and validate suitable microstructural models.

2. Materials and methods

2.1. Ethical approval

The study was exempted from ethical committee review according to national regulations (German Animal Welfare Act), as porcine muscles of healthy, female domestic pigs were obtained from a slaughterhouse immediately after animal sacrifice.

2.2. Sample preparation

Within this study hind legs ($n = 10$) of female domestic pigs (*Sus scrofa domestica*) were obtained from a slaughterhouse immediately after animal sacrifice. Legs were transported in a cooling box to the laboratory, where the unipennate biceps femoris muscle, see also Remark 1, was excised and stored at 4◦C in a climatic chamber wrapped in physiological solution (NaCl, 0.9%) soaked cloths. For the tissue scale experiments ten ($n = 10$) tissues samples (tension: $n = 5$, compression: $n = 5$), see Table 1, were cut with respect to their fibre orientation (fibres were oriented parallel to the loading direction). Their dimensions were chosen to facilitate testing on the one hand, and to obtain samples that are representative of the tissue in terms of the fractions of ECM and muscle fibres. Alginate was used to stabilise the tissue during cutting [8]. After the tissue strips were dissected from the outer region of the muscle, axial tension and compression experiments were performed at room temperature, see Section 2.3.

From the same muscle type twelve ($n = 12$) intact muscle fibres (tension: $n = 7$, compression: $n = 5$), see Table 2, were dissected by forceps, and placed in muscle relaxing solution composed of EGTA (7.5 mM), potassium propionate (170.0 mM), magnesium acetate (2.0 mM), imidazole (5.0 mM), creatine phosphate (10.0 mM), ATP (4.0), leupeptin (17.0 µg/ml), and E64 (4.0 µg/ml) at room temperature to prevent protein degradation. For the mechanical fibre experiments only fibres without any amount of endomysium were considered. While the fibres used for axial tension experiment needed no further processing, fibres for the axial compression tests were cut into segments using femtosecond laser technology, for details see Böl et al. [61]. Thereby the height-to-diameter ratio was maintained at ≤ 1, to avoid buckling of the sample during loading.

Remark 1 ((Muscle selection).)**.** The use of the biceps femoris muscle within the present study has different advantages: At first, it is a unipennate muscle, which allows preparing a larger number of tissue samples with clear, identical fibre orientation. Furthermore, the muscle is relatively large, which leads to a large number of specimens per muscle. Finally, this muscle is located directly under the skin, which simplifies and speeds up the preparation. Together with the immediate availability of the legs after slaughter and a short distance to the laboratory this helps performing experiments as close as possible to the in-vivo situation, as is in the previous studies [8,9,34,64,65].

Table 1
Number and dimensions of tissue scale samples. The indices t and c define the samples for tension and compression experiments. Further, L, H_c, $W_{t/c}$, and $T_{t/c}$ define the sample length, height, width, and thickness of the dissected sample, respectively. L_t denotes the distance between the clamps in tension experiments, cf. Fig. 1 (a).

	sample no. [-]	L [mm]	L_t [mm]	W_t [mm]	T_t [mm]	H_c [mm]	W_c [mm]	T_c [mm]
axial tension	I	61.6	30.8	12.1	4.6	-	-	-
	II	61.4	30.7	12.7	4.7	-	-	-
	III	60.9	30.4	10.3	4.3	-	-	-
	IV	60.8	30.3	10.2	3.8	-	-	-
	V	60.0	30.3	11.7	4.2	-	-	-
axial compression	VI	-	-	-	-	10.0	8.9	11.1
	VII	-	-	-	-	11.1	9.3	10.7
	VIII	-	-	-	-	9.3	9.6	10.0
	IX	-	-	-	-	10.6	8.8	10.9
	X	-	-	-	-	9.7	8.3	10.8
mean ±s.d.		**60.9±0.6**	**30.5±0.2**	**11.4±1.0**	**4.3±0.3**	**10.1±0.6**	**9.0±0.4**	**10.7±0.4**

Table 2
Number and dimensions of fibre scale samples. A, l, and h denote the cross-sectional area, length, and height of the fibre samples. cf. Fig. 2 (b).

	sample no. [-]	A [μm^2]	l [μm]	h [μm]
axial tension	XI	14478	1150	-
	XII	11367	1070	-
	XIII	15158	944	-
	XIV	9374	560	-
	XV	10339	570	-
	XVI	20778	1060	-
	XVII	15184	640	-
axial compression	XVIII	12565	-	93
	XIX	17884	-	190
	XX	18132	-	187
	XXI	15985	-	113
	XXII	14957	-	134
mean ±s.d.		**14683±3216**	**856±238**	**143±39**

2.3. Mechano-optical experiments at tissue and fibre scales

Muscle tissue specimens and sections of single fibres were tested mechanically and monitored by optical measurement systems. Like most soft biological tissues skeletal muscle shows preconditioning effects during ex-vivo mechanical testing, i.e., the response becomes repeatable only after a few load cycles, see e.g. Ahamed et al. [66]. The comparability of tissue and fibre scale responses would therefore require 'matching' pre-conditioning protocols, i.e., single fibres should be subjected to the same preconditioning history as fibres embedded in the tissue, which can hardly be ensured. Therefore, the mechanical responses of both fibres and tissue were analysed during the first loading.

2.3.1. Tissue scale experimental investigations

At tissue scale, defined here as the length scale of about one centimetre, axial tension and compression experiments were performed using an axial testing machine (Zwick Z010, Zwick GmbH & Co. Ulm, Germany). The specific setups are illustrated in Fig. 1. In order to perform the axial tension experiments, the strips, whose fibres were oriented parallel to the loading direction, were fixed in clamps covered with sandpaper from the inside to avoid tissue slippage, see (a). Tension experiments were carried out until the sample failed. For performing the compression experiments (with fibre orientation parallel to the loading direction), tissue samples were positioned between two polytetrafluoroethylene plates. While the lower one was fixed, the upper was installed on the force sensor which in turn was fixed to the movable cross beam. Before placing the samples between the plates, they were sprayed with silicon oil to avoid friction. The specimens were deformed until a maximum compressive strain of 50%. It should be noted at this point, that this compression level is in the physiological range. E.g., isokinetic contraction experiments show a 25% global muscle belly shortening, local compression levels on the same muscle surface, which were determined using optical measuring systems, even show compression levels of around 50% [67], where both compressive strain levels (25% and 50%) are measured with respect to the inactive, passive muscle belly situation.

In accordance with previous experimental investigations [8,9], and thus to ensure comparability, all tissue scale experiments were performed at a strain rate of $\dot{\varepsilon} = 0.5\%\,s^{-1}$. This rate is clearly lower than in the case of active muscle contractions. For passive loading situations that occur, e.g., when sitting, touching, etc., the strain rate used is in a relevant range. While the displacement U of the upper movable cross beam was prescribed, the force F was measured and converted to mean engineering stress via $P = F/A$, where A is the undeformed tissue strips cross-sectional area. Further, the axial stretches $\lambda_t^{tiss} = 1 + U/L_t$ and $\lambda_c^{tiss} = 1 - U/H_c$ for tension and compression experiments, respectively, were calculated from the magnitude of displacement U and the undeformed sample length L_t and height H_c. After examination of the data, it was reduced in accordance with Section 2.4.

Since a major objective of this study is the determination of tissue volumes during deformation, samples were coated with fine white and black varnish before placement in the measurement setup. A previous study [67] had shown that the varnish does not influence the mechanical properties. During the experiment, the tissue surfaces were recorded using 4 optical measuring systems positioned around the sample, each consisting of 2 CCD cameras with a recording frequency of 1 Hz. Each camera provides 8-bit images with a resolution of 2352 × 1728 (pixel size: 0.05 mm) and 2048 × 2048 (pixel size: 0.03 mm) in TIFF- and PNG-format. Based on a calibrated marker pattern and the random patterns on the sample surfaces, the three-dimensional surface of the samples can be reconstructed in a post-processing step, see Fig. 4, a procedure that has been frequently realised by the authors [17,67,68]. In doing so, for the axial tension and compression experiments volumes were determined at several stretch levels.

2.3.2. Fibre scale experiments

For fibre scale experiments, a micromechanical setup was embedded within an inverted microscope, see Fig. 2. All fibre scale experiments were performed in a basin filled with muscle relaxing solution, see Section 2.2, to prevent dehydration.

Following Table 2, seven ($n = 7$) axial tension experiments were performed. While one end of the fibre was glued to a movable plastic plate, the other end was glued to a fixed platform. The movable plate was connected via a fine copper wire to a force sensor attached to a piezoelectric-driven micro manipulator, see Fig. 2 (a),

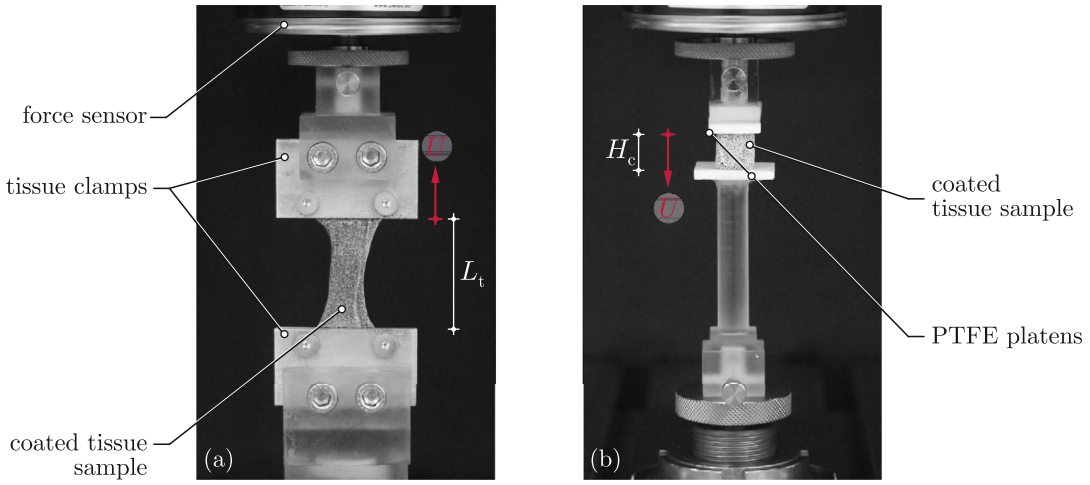

Fig. 1. Experimental setups for tissue scale (a) axial tension and (b) compression experiments.

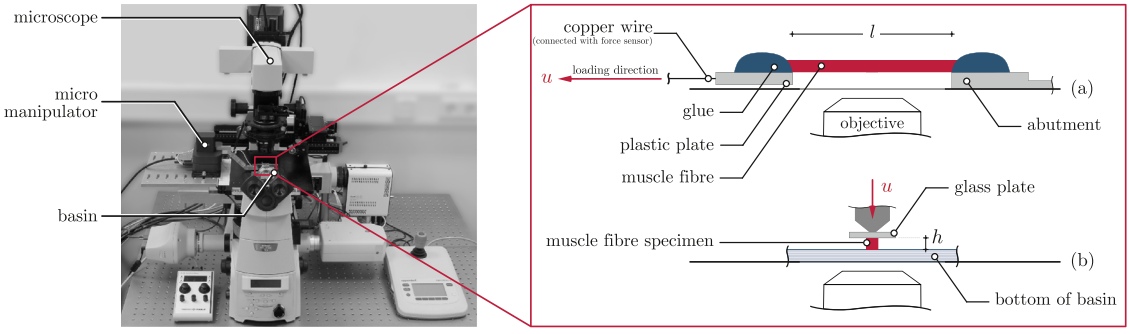

Fig. 2. Fibre scale experimental setup: Experimental configuration for (a) axial tension and (b) compression experiments. For a real photographs of the experimental setup, see also Supplementary material.

allowing the stretching of the fibre while measuring the length change and the force. For more details see also Böl et al. [61]. By pulling the fibre up to a pre-load of 1 µN, the fibre was aligned horizontally, defining the reference length l, see (a). In this situation, a three-dimensional image stack was acquired by confocal laser scanning microscopy (CLSM), allowing the determination of the fibre's cross-sectional area A. While during the experiments the displacement u was specified, the force response F was measured and converted to mean engineering stress via $P = F/A$. Finally, the axial stretch $\lambda_t^{fib} = 1 + u/l$ was calculated using u and l.

For the realisation of five ($n = 5$) axial compression experiments, the trimmed fibre segments were positioned upright within the basin filled with relaxation solution, see Fig. 2 (b). A square glass plate was glued at the tip of the force sensor, which was connected to the micro manipulator. Fibre segments were compressed until a pre-load of 0.5 µN was attained. Based on the generation of CLSM three-dimensional image stacks, the initial heights h and the cross-sectional areas A of the muscle fibre segments were determined, see Table 2. During the deformation driven experiments, the displacement of magnitude u was specified and the responding force F was measured. In a following step the mean engineering, compressive stress was calculated via $P = F/A$. Finally, the compressive stretch $\lambda_c^{fib} = 1 - u/h$ was calculated using u and h.

After performing both the tensile and compression tests, the data were checked and reduced according to Section 2.4.

Volume determination at fibre scale was based on CLSM images stacks recorded before applying mechanical deformation and bright-field observation during the mechanical tests. For typical reconstruction in axial tension and compression, see also Supplementary material. After the pre-load in both deformation states were reached CLSM image stacks were recorded, directly providing the three-dimensional geometry. During continuous deformation (tension/compression) the recording of CLSM stacks is impossible. Consequently, bright-field recordings allow to inform about the width (axial tension) and the diameter (axial compression) of the fibre, from which in turn the volume was calculated in a post-processing step, see also Böl et al. [62].

2.4. Data processing

The tissue scale axial tension raw data in form of force-displacement relations include a large number of measuring points. In order to make the data manageable, raw data underwent three processing steps: First, we set a pre-stress of 0.07 kPa (to be the smallest possible pre-stress at tissue and fibre level) for the tensile and compression tests. Compared to the literature, this pre-stress is relatively small, which is important for comparing the tissue and fibre data. We note that these preloads were subtracted from the stress when plotting the results unless stated otherwise. Secondly, all raw data were smoothed and the number of data points was reduced. Finally, the elastic regions of the stress-displacement curves were determined by successively computing tangents $\mathcal{T}_i$ by finite differences at the points U_i, $i = 1, 2, ..., m$, where m indicates the maximum number of measuring points. The elastic range of the curve was then defined as the region where the slope is monotonically increasing, i.e., where $\mathcal{T}_{i+1} \geq \mathcal{T}_i$. The point u_j at which $\mathcal{T}_{j+1} < \mathcal{T}_j$ marks the end point of the elastic region. We note that $\mathcal{T}_i$ is an indicator of the stretch-dependent stiffness.

Analogous to the tissue experiments, the pre-stress for both deformation states (tension/compression) in fibre-scale tests was set

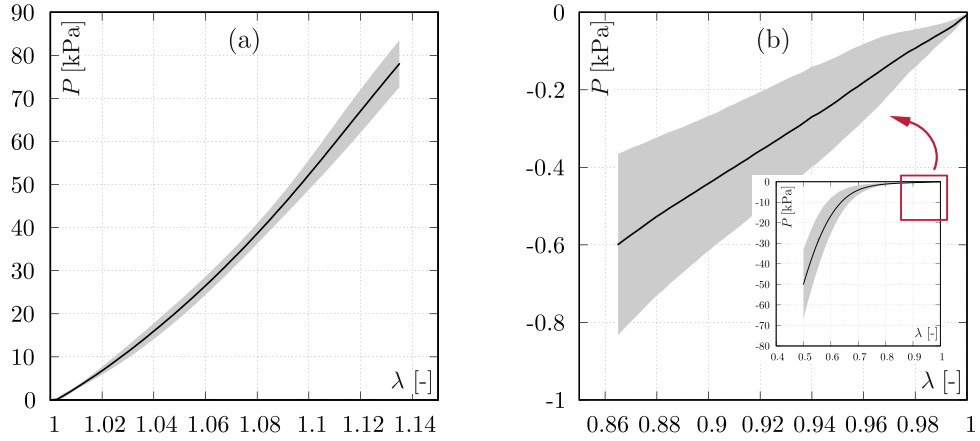

Fig. 3. Tissue scale stress-stretch responses of (a) axial tension and (b) axial compression experiments. Solid curves indicate mean values and shaded areas depict the standard deviations.

to 0.07 kPa. Thereafter, raw data were smoothed using a moving average filter with a span length of 5 data points. Cubic spline interpolation was used at 250 strain points with a step size of 0.2% for each data set, resulting in a total of 500 data points in a single cycle. Mean values and standard deviations were then calculated from the interpolated forces. All processing steps were performed with custom-made Matlab scripts (Matlab® R2017a, The MathWorks, Inc.).

We remark that all samples were examined for damage after the test had been carried out and measurements were discarded from the analysis if they could not be evaluated due to operational disturbances (e.g. slipping of the specimen under compression or unintentional shift of the camera) and tearing of the specimens in the clamping region during tension experiments. Overall, $n = 8$ samples were discarded.

2.5. Statistics

To prove whether there are statistical differences between the deformed volumes and the original volume for the tissue and fibre scale specimens, under both axial tension and compression, the unpaired Mann-Whitney U-test was applied. This tested the null hypothesis that the mean values of the measured deformed and original volumes are equal at a significance level of $\alpha = 0.05$.

3. Results

3.1. Axial tension and compression experiments at tissue scale

The mean stress-stretch responses of the axial tension and axial compression experiments at tissue scale are provided in Fig. 3 as solid curves, and the shaded areas represent the standard deviations. In order to provide mean values and standard deviations from all tension samples, the stretch range up to $\lambda_t^{tiss} = 1.135$ shown in (a), corresponds to the smallest elastic region among the tested samples. In the following, this value is called λ_a for all tensile experiments ($\lambda_a = 1.135$) and compression experiments ($\lambda_a = 0.865$), regardless of whether tissue or fibres are tested. The maximal standard deviations consistently occurred at the maximum stress values. Expressed as percentages of the corresponding mean values (s.d./mean $\times$ 100), i.e., coefficients of variation, they reach 30% at λ_a and 34% at maximum stretch for the axial tension compression tests, respectively. For biological tissues, these relatively small standard deviations indicate the satisfactory reproducibility of the experiments. Additionally, the exponential-like nature of the stress-strain response in case of the compression experiments (subfigure in Fig. 3 (b)) reveals non-linear behaviour, similar to that of the majority of soft tissues. While this non-linear behaviour is clearly expressed for the compression experiments (b), the axial tension experiments (a) show a much less pronounced non-linear behaviour. Further, evaluating the stresses at λ_a features an approximately 130-fold higher stress value in tension than in compression, which suggests a strong TCA if defined on the interval $\pm$ 0.135 stretch interval. For a direct comparison of the stress-stretch curves we refer to the supplementary material, see also Supplementary material.

In addition, the volume changes $J = V/V_0$, where V is the deformed volume and V_0 denotes the initial volume, were determined at discrete stretch values (tension: $\lambda_t^{tiss} = 1/1.045/1.09/1.135$; compression: $\lambda_c^{tiss} = 1/0.955/0.91/0.865/0.9/0.8/0.7/0.6/0.5$) for all samples. Representative three-dimensional examples of the axial tension (a) and axial compression state (b) are shown in Fig. 4. The mean volume change-stretch responses of the axial tension and axial compression experiments are provided in Fig. 5. The maximal standard deviations consistently occurred at the maximal deformation values and were 2.5% and 1.4% for the axial tension and compression tests, respectively. Volume increase was observed under tensile loads and volume reduction was recorded under compressive loads. Albeit significant, these volume changes were small and the mean varies on the order of 1 to 2% in the symmetric strain range of about $\pm$ 14% ($J = 1.016$ at $\lambda_t^{tiss} = 1.135$ and $J = 0.99$ at $\lambda_c^{tiss} = 0.865$). Although the volume changes become larger for higher compressive loads, even at 50% axial compression the volume reduces only by 4%. As a consequence, and in view of the observed standard deviations, very weak compressibility can be attributed to the tissue scale behaviour in both deformation states.

3.2. Axial tension and compression experiments at fibre scale

At fibre scale the samples were loaded by a maximum of 50% in tension and compression. The stress-stretch relations are illustrated in Fig. 6. The maximal standard deviations consistently occurred at the maximal stress value and were 29% and 53% for the axial tension and compression tests, respectively. Non-linearity of the stress-stretch curve is more pronounced for the compression response. Notably, the evaluation of both deformation states at 50% deformation reveals approximately 14-fold higher stresses under tension than compression, documenting strong TCA if evaluated at the $\pm$ 0.5 stretch interval. For comparison with the tissue-scale experiments the ratio of tensile to compressive stresses was

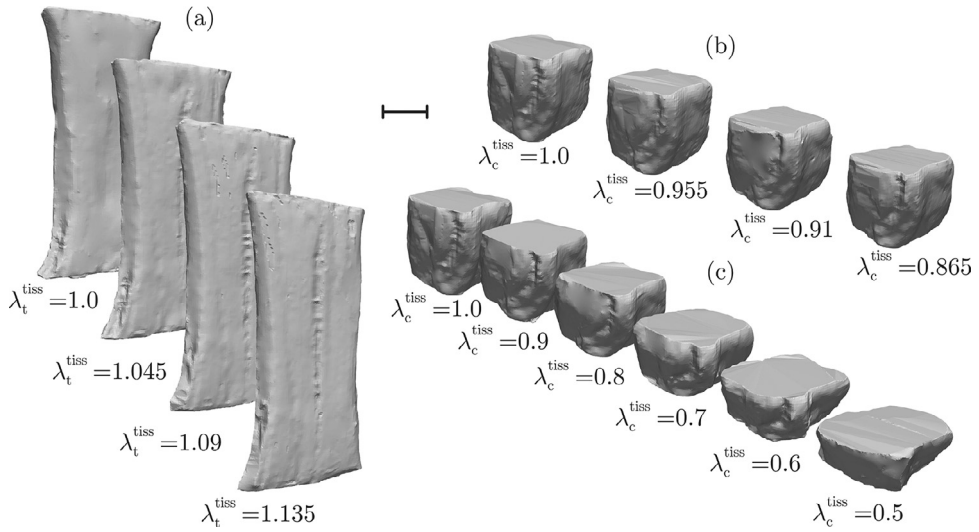

Fig. 4. Illustrative example of three-dimensional, reconstructed tissues samples: (a) Axial tension (sample XVII, see Table 2) and (b) axial compression deformation (sample XX, see Table 2) reconstructed at discrete stretch levels of $\lambda_t^{tiss} = 1/1.045/1.09/1.135$ and $\lambda_c^{tiss} = 1/0.955/0.91/0.865$, respectively. Scale bar: 5 mm.

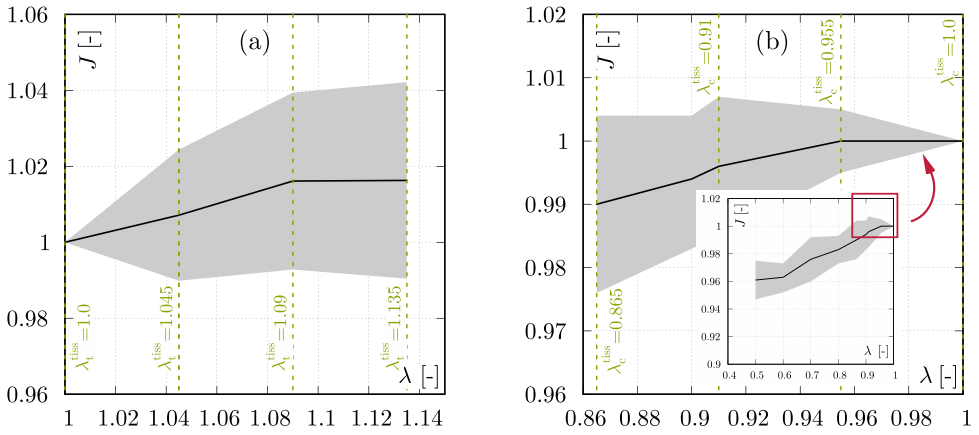

Fig. 5. Volume changes during (a) axial tension and (b) compression tests at tissue scale. For the axial tension and compression experiments volumes at discrete stretch levels $\lambda_t^{tiss} = 1/1.045/1.09/1.135$ and $\lambda_c^{tiss} = 1/0.955/0.91/0.865$ were determined, respectively, see also Fig. 4. Solid curves indicate mean values, and the shaded areas depict standard deviations. To guide the eye, data points were connected by lines. The differences between the deformed state volumes and the referential volume at $\lambda^{tiss} = 1$ were significant for all levels.

also evaluated at λ_a, providing a TCA ratio of approximately 6. The comparison with the corresponding tissue value of 130 reveals a clear difference between the TCA at the two scales. Finally, the volume changes for both deformation states at fibre scale were determined and are illustrated in dependence of the axial stretch in Fig. 7. Remarkably, in terms of the mean values of J, the data indicate a statistically significant reduction of volume under both tensile and compressive loads in the order of 5% and 9% at λ_a for tensile and compressive loads, respectively. For increased loads, the trend is less clear under tension, whereas under compression the volume reduces monotonically by more than 30% at $\lambda_c^{fib} = 0.5$.

4. Discussion

4.1. Tissue mechanical properties

Basically, most investigations at tissue level were performed as axial tension [10–16,31,32,69–76] and compression experiments [8,9,17,19,21–24,31,32,72,77]. Muscle tissue from various species were mechanically tested, including pigs [e.g. 8,9,17,21], chicken [32], cattle [16,22,76], rodents [10,12,13,69,73,75], and humans [11,70,71,74]. Before passive mechanical testing, the tissues were subjected to various mechanical and thermal processes. E.g., while in some cases cadaveric tissue was chosen [71,74] or the tissue was frozen before sampling and then thawed again for the actual mechanical testing [e.g. 11,13,70], in other studies the tissue was sampled as soon as possible after dissection [e.g. 8,17,22] to be as close as possible to the in-vivo situation. A further parameter that influences the passive mechanical properties of muscles is temperature. E.g., Noonan et al. [78] described higher linear stiffness, lower deformation, and higher failure load of the specimen at lower temperatures for rabbit skeletal muscles. Another important factor that clearly influences the mechanical material response is the loading rate, which varies between $0.001\%\,s^{-1}$ [19] and $37,800\%\,s^{-1}$ [21]. Finally, the starting point of the stress-strain relation significantly influences the maximum stress but also the elastic region of the stress-stretch relation. There are also different approaches to this in the literature. Some studies do not use a pre-load [e.g. 13,73,75], while others choose it arbitrarily [e.g. 11,71,72] or depending on the mass of the tissue samples [21]. It is therefore not surprising that the results obtained in these studies strongly depend on the different protocols and vary accordingly.

In Fig. 8, the maximum stresses reached at λ_a of the tensile (a) and compressive (b) stretch range from approximately 4 kPa [16] to 87 kPa [11] and -0.2 kPa [23] to -1.4 kPa [72], respectively.

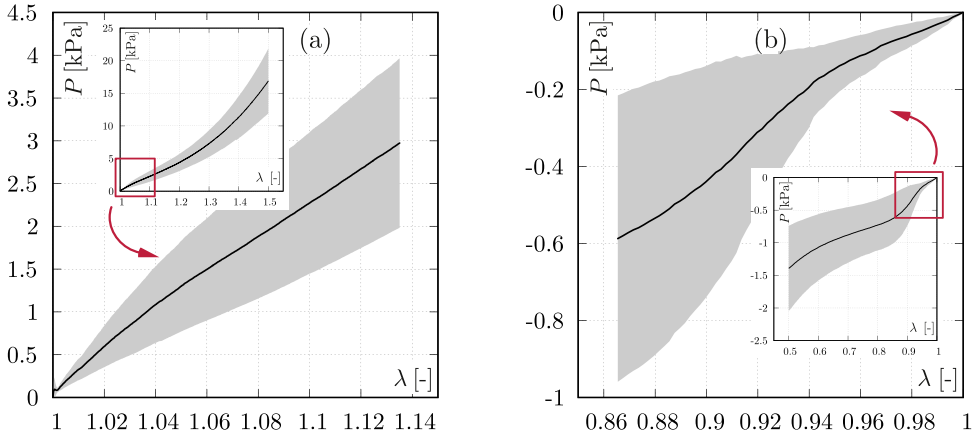

Fig. 6. Fibre scale stress-stretch responses of the (a) axial tension and (b) compression experiments. Solid curves indicate mean values and shaded areas depict the standard deviations.

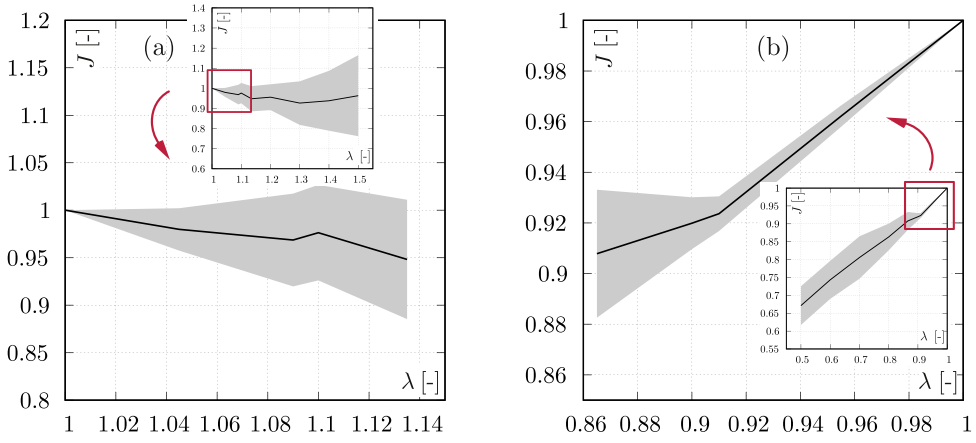

Fig. 7. Volume changes during (a) axial tension and (b) compression experiments at fibre scale, evaluated at six discrete stretch levels (tension: $\lambda_t^{fib} = 1/0.955/0.91/0.9/0.865/0.8/0.7/0.6/0.5$, compression: $\lambda_c^{fib} = 1/1.045/1.09/1.135/1.2/1.3/1.4/1.5$). The solid curves indicate mean values, and the shaded areas depict standard deviations. The differences between the deformed state volumes and the referential volume at $\lambda^{tiss} = 1$ were significant for all levels.

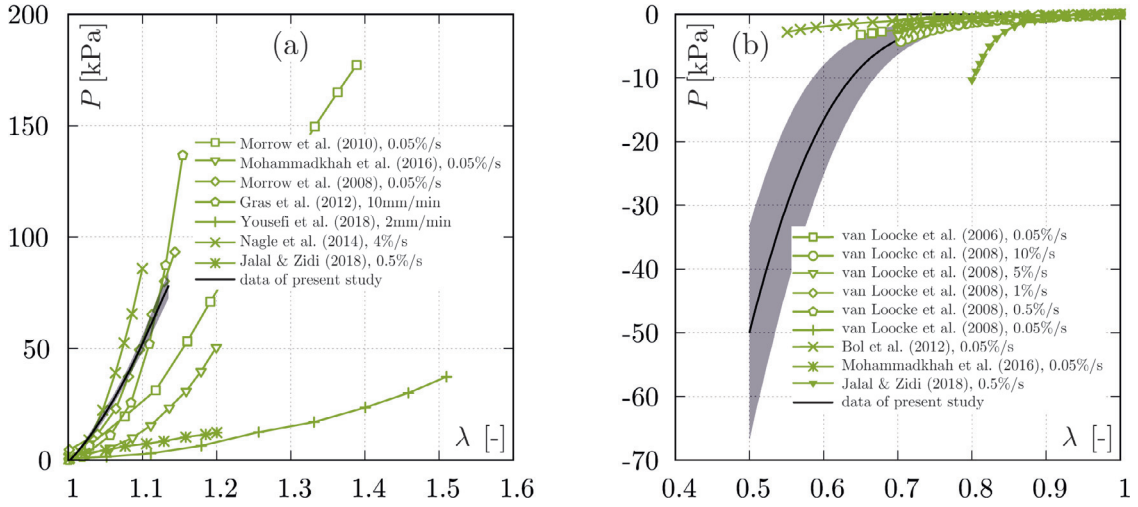

Fig. 8. Comparison to literature: (a) Tension and (b) compression experiments. Note, only experiments with loading rates between 0.05% s^{-1} and 10% s^{-1} were considered, as this are close to the loading rate of 0.5% s^{-1} used in the present study.

The mean tensile and compressive stresses of 78 ± 5.4 kPa and -0.6 ± 0.2 kPa, respectively, in the present study thus fall within the range of the values reported in the literature. We restricted the analysis in this study to the common (and thus the smallest) elastic region of the tensile response among all tested samples. The minimum marks $\lambda_a = 1.135$, cf. Fig. 8 (a), and the mean values is 1.16 ± 0.01. The elastic range clearly ends before failure occurs. This is consistent with rupture stretches of 1.24 ± 0.14 that were evaluated from a selection of studies [11,13,16,32,72–74]. The small standard deviation of 0.01 in the stretch that marks the elastic range suggests that the determination of this value as described in Section 2.4 works robustly, and that this value could be used as a conservative alternative to the rupture stretch for determining the critical, and possibly supra-physiological strain regime.

4.2. Fibre mechanical properties

While, except from recent contributions by some of the authors [61,62], muscle fibres have so far exclusively been tested in axial tension, muscle fibres were both extended and compressed axially in the present work. In comparison to the different experimental protocols for tissue scale testing, see Section 4.1, the variations among testing protocols for single fibres is distinctly greater. This is reflected by the results of these studies and complicates a quantitative comparison of our data with the literature in analogy to the tissue-scale data shown in Fig. 8, see also Böl et al. [61]. In fact, the reported passive stresses for axial tension experiments vary between 5 kPa [36,38,45] and 100 kPa [39,54] at a maximum deformation of 50%. Notwithstanding, the reached maximum tension stress of 16.9 ± 5.0 kPa achieved in the present study, see Fig. 6 (a), is within the range of these values found in the literature. Given the lack of literature data, a comparison of the compressive stresses is not possible.

4.3. Tension-compression asymmetry at tissue and fibre level

Several soft biological tissues such as tendon [79], cartilage [80], bone [30], lung tissue [26], brain [27], or cervical tissue [29,81] exhibit significantly different behaviour under passive tensile and compressive loads, respectively, a property referred to as TCA. This also applies to muscle tissue [e.g. 8,9,22,32,82]. Gindre et al. [82] compared experimental porcine compression data from van Loocke et al. [22] with tension data from Takaza et al. [15], while Mohammadkhah et al. [32] focussed on compression and tension data of chicken muscle tissue. Regardless of the species and the direction of loading considered, it was found that the stress-strain response under tension loading is approximately two orders of magnitude larger than the response under compression loading. While Gindre et al. [82] and Takaza et al. [15] reported on TCA at a discrete selection of strains, we provide here continuous data that show the development of TCA during the deformation process. In Fig. 9 (a), the ratio $P_t/|P_c|$ between the magnitudes of tensile P_t and compressive tissue stress $|P_c|$ is illustrated in dependence on the absolute strain $|\varepsilon|$, with a maximum at 0.135%. The degree of TCA increases with increasing deformation and consequently strongly depends on the deformation. At the maximum strain of 13.5% the 130-times higher tensile stress lies within the region of two orders of magnitude reported by Gindre et al. [82] and Takaza et al. [15].

Fig. 9 (b) illustrates the development of fibre scale TCA. Overall, a non-linear relationship is observed over the entire deformation range of 50%, see subfigure. For small strains around 1%, the TCA ratio is about 22 and continuously drops to a minimum about 6 at $\varepsilon = 0.135$. Thereafter it rises again and reaches a value of about 14 at maximum deformation of $\lambda_c^{fib} = 0.5$. This non-monotonicity reflects differences in non-linearity between the tension and compression behaviour, but we note that beyond the elastic range marked by $\varepsilon = 0.135$, inelastic effects may also play an increasing role, and lead to the existence of a minimum.

The comparison of asymmetries on different scales provides insight on the role of the different tissue components of composing the tissue-scale mechanical response. In this study, muscle fibres and tissue were taken from the same muscle and species, allowing for a direct comparison. The TCA at tissue scale is more than 22 times more pronounced than at fibre level, and although the reason for this large difference in TCA remains speculation, the differential consideration of tissue and fibres in our study strongly points at a distinct role of the complementary ECM components in magnifying or even causing this phenomenon in its full extent. The ECM structures the tissue hierarchically and may therefore be responsible for the generation of intricate deformation mechanisms within the muscle tissue [64,65]. On the one hand, the ECM embeds the muscle fibres in an only approximately straight and rather wavy shape, see Kuravi et al. [64]. As a consequence, tissue compression in fascicle direction may not directly be translated into axial compression of the fibres by the same amount, but elicit a structural response, e.g., with increased waviness and thus different axial deformation of the fibres. On the other hand, skele-

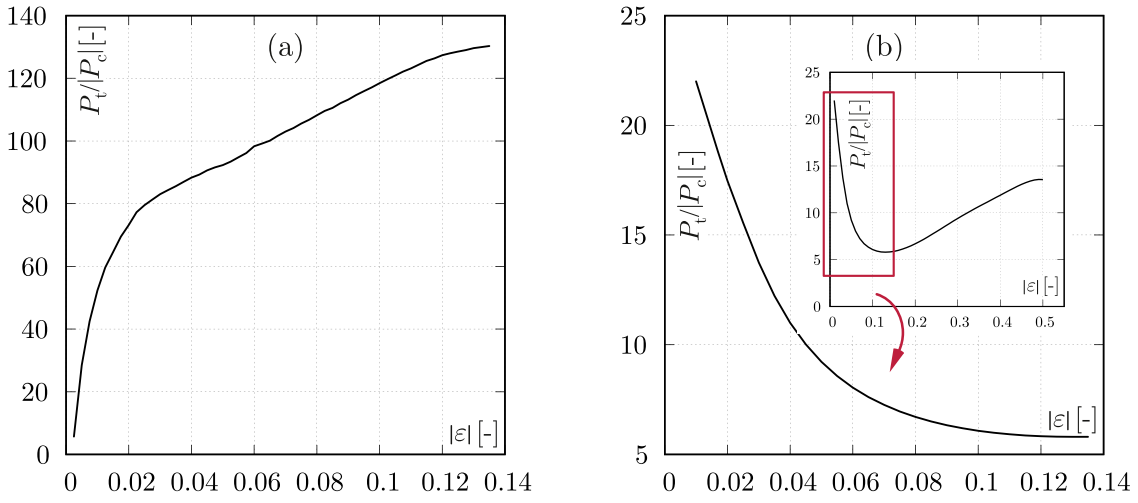

Fig. 9. Development of TCA for (a) tissue scale and (b) fibre scale experiments.

tal muscle ECM is highly organised, hierarchically structured, and forms anisotropic collagenous envelopes around muscle fibres (endomysium) and groups of them (perimysium), see e.g. the summary in Böl et al. [8]. Given the network-like structure of these thin sheaths, a pronounced difference in their responses to tensile and compressive loads is expected that may be observed at the tissue length scale. This hypothesis is supported by experimental studies that report different reorganisation of the perimysial collagen under tension and compression loads [31,35]. Direct experimental validation, however, is lacking. Although isolated muscle ECM has been tested in axial tension and lateral compression [34], the loose and floppy structure of this material makes reliable axial compression tests hardly possible.

4.4. Volume changes

Due to their high intra- and extracellular water content, biological tissue is frequently considered as an incompressible, i.e., volume-preserving material, particular in the context of constitutive modelling [83–92], although there is an active ongoing discussion on this topic in the literature. Towards addressing the question of load induced volume changes, the surfaces of the deforming specimens need to be tracked and reconstructed, which generally poses a challenge in the experimental set-up. In the present study, this was achieved with either four sets of cameras, cf. Fig. 4, or by use of combined CLSM and brightfield microscopy. The corresponding volume changes are shown in Figs. 5 (tissue scale) and 7 (fibre scale). The results indicate that the tissue is compressible at both length scales, even if the scatter in this data is high. Moreover, the compressibility of the volume changes at tissue scale are low and, even under severe compressive load of 50% compressive strain, the volume merely reduces by 5%. The muscle fibres underwent higher volume changes, at 50% compression, e.g., the volume reduction amounts to 33%, about a factor of 24 times higher the corresponding tissue value. Surprising is the 'inverse' volumetric behaviour observed for muscle fibres under tensile load, which show a trend to reduce their volume (by about 5% at $\lambda_a = 1.135$) in the initial phase of extension, although the state of hydrostatic tension implied by a uniaxial tension test would suggest an increase in volume with tension for a 'common' compressible material, see e.g. Ogden [93, p. 223] or the supplementary information in Ehret et al. [94]. The observed, seemingly unusual, characteristic known as 'negative compressibility' does not contradict thermodynamic principles [95] and is even covered by isotropic nonlinear elasticity theory; it has been observed in many soft biological tissues, and could be explained in terms of their microstructure [94]. Nevertheless it is still a surprising feature, which is consistent with slight, albeit insignificant volume losses reported by Smith et al. [63]. The reason for the notably higher compressibility at fibre level is unknown so far. The analysis is beyond the scope of the present study, although the high level of intracellular organisation within the sarcomere compartments of the muscle fibres suggests itself as a candidate to explain this behaviour.

Notably the fibres are embedded within the ECM, in particular the endomysium, and the fascicles in turn are surrounded by the perimysium. The differential consideration of tissue and fibre response therefore suggests that the ECM must play a key role in establishing the near volume preservation, either by constraining and thus preventing the fibres from undergoing volume changes, by compensating the fibres' volume reduction through volume increase, or by a combination of both effects. In fact, an exchange of liquid between the highly hydrated tissue components as a result of deformation, in particular between muscle cells and ECM, seems plausible. The structural mechanisms that allow this load sharing, and the potential role of fluid exchange between fibres and ECM remain unknown to date and are beyond the scope of the present work.

4.5. Impact on muscle modelling

In addition to a better understanding of load transfer mechanisms in muscle tissue, the data collected here in the form of classical stress-stretch graphs and new volumetric data recorded during loading are of great interest and provide valuable information for the development of reliable concepts to model the mechanical response of skeletal muscle tissue. Except for a few studies by the authors [61,62], there is a general lack of fibre scale compression experiments. Information on the passive compressive behaviour of muscle fibres, required to understand the fibres' mechanical response over the entire range of in-vivo strains, which includes the phenomenon of TCA, is therefore largely missing. For micromechanically inspired models, however, that distinguish between the contributions of fibres and ECM to the overall response, this information is key. The results generated here therefore not only allow the development of modelling approaches to describe the phenomenon of TCA at tissue and fibre scale, but also help refining the typical assumptions on fibre compressive properties in existing models.

In addition, the volumetric data allow conclusions about fluid exchange mechanisms on tissue and fibre level, which can serve as a basis for the development of bi-phasic, poro-elastic models [e.g. 96] specific for muscle tissue, as suggested in Simms et al. [97]. While weak compressibility or even incompressibility may be an acceptable assumption when modelling skeletal muscle at the tissue scale, the adoption of these concepts for the single components may fail. The drastic compressibility of muscle fibres and large compressive loads, and their negative compressibility at low tensile loads seem to be characteristics features, and point at complex interactions between ECM and muscle fibre that need to be understood. Potentially, the different volumetric characteristics between fibres and tissue can only be fully explained when employing multiphasic models that account for the exchange of fluid between the tissue components upon deformation.

In constitutive models of skeletal muscle tissue, one strategy to achieve TCA is based on neglecting the mechanical contribution of the muscle fibres under compression [e.g. 98,99]. The presented results, however, challenge this strategy, as the more pronounced TCA at tissue level points at an even stronger TCA contribution of the ECM on the one hand, and the small difference between the compressive responses of muscle fibres and tissue in the range $[\lambda_a, 1]$ indicates a notable contribution of the muscle fibres to the tissue stress on the other hand. Notwithstanding, existing modelling frameworks and, in particular, computational models that take account of the tissue microstructure [e.g. 64,65,100–103] may have the capacity to capture the observed behaviour and to unravel the mechanisms of load transfer when informed and improved through component-level data as provided in the present study.

5. Conclusion

The present work analysed and compared the TCA displayed by skeletal muscle at tissue and fibre scale. In addition, the volume changes of tissue and fibre specimens with application of passive tensile and compressive loads were studied: Both TCA and the volumetric behaviour differ between the tissue and fibres. TCA is much more expressed at tissue scale. The tissue shows little compressibility and only increases the volume slightly upon uniaxial tension and reduces it with compression. The fibre, on the other hand, decreases the volume both under uniaxial tension and compression and undergoes large volume changes under higher com-

pressive loads. Although not subject to individual testing in the present work, this study identifies a key role of the ECM in establishing the mechanical response of skeletal muscle tissue: It contributes significantly to the passive stress, it is responsible for the major part of tissue-scale TCA either directly through its material properties, or indirectly by embedding the muscle fibres, and most probably prevents or balances the volume changes of muscle fibres during deformation. The new results contained in this study thus shed light on the origin of TCA and provide new information can be used in microstructure-based approaches to model and simulate skeletal muscle tissue.

Declaration of Competing Interest

The authors declare that they have no known competing financial interests or personal relationships that could have appeared to influence the work reported in this paper.

Acknowledgments

This work was supported by the Deutsche Forschungsgemeinschaft (DFG) under Grants 320032210 and 258667461, and the Swiss National Science Foundation (SNSF) under Project No. 169870. AEE thanks R. Kuravi (Empa) for helpful discussions on the effect of pre-stresses on data evaluation.

Supplementary material

Supplementary material associated with this article can be found, in the online version, at doi:10.1016/j.actbio.2022.03.034.

References

[1] I. Janssen, S.B. Heymsfield, Z. Wang, R. Ross, Skeletal muscle mass and distribution in 468 men and women aged 18–88 yr, J Appl Physiol 89 (1) (2000) 81–88.
[2] T. Abe, S.L. Buckner, S.J. Dankel, M.B. Jessee, K.T. Mattocks, J.G. Mouser, J.P. Loenneke, Skeletal muscle mass in human athletes: what is the upper limit? Am J Hum Biol 30 (3) (2018) e23102.
[3] M.C. Dalakas, Inflammatory muscle diseases, N Engl J Med 372 (18) (2015) 1734–1747.
[4] R. Furrer, C. Handschin, Muscle wasting diseases - novel targets and treatments, Annu Rev Pharmacol Toxicol 59 (2019) 315–339.
[5] E.M. McNally, P. Pytel, Muscle diseases - the muscular dystrophies, Annu Rev Pathol: Mech Dis 2 (1) (2007) 87–109.
[6] L. Larsson, H. Degens, M. Li, L. Salviati, Y.L. Lee, W. Thompson, J.L. Kirkland, M. Sandri, Sarcopenia - aging-related loss of muscle mass and function, Physiol Rev 99 (1) (2018) 427–511.
[7] P.N. Siparsky, D.T. Kirkendall, J.R. w. E. Garrett, Muscle changes in aging - understanding sarcopenia, Sports Health 6 (1) (2014) 36–40.
[8] M. Böl, A.E. Ehret, K. Leichsenring, C. Weichert, R. Kruse, On the anisotropy of skeletal muscle tissue under compression, Acta Biomater 10 (7) (2014) 3225–3234.
[9] M. Böl, K. Leichsenring, M. Ernst, A.E. Ehret, Long-term mechanical behaviour of skeletal muscle tissue in semi-confined compression experiments, J Mech Behav Biomed Mater 63 (2016) 115–124.
[10] B. Calvo, A. Ramírez, A. Alonso, J. Grasa, F. Soteras, R. Osta, M.J. Muñoz, Passive nonlinear elastic behaviour of skeletal muscle - experimental results and model formulation, J Biomech 43 (2) (2010) 318–325.
[11] L.L. Gras, D. Mitton, P. Viot, S. Laporte, Hyper-elastic properties of the human sternocleidomastoideus muscle in tension, J Mech Behav Biomed Mater 15 (2012) 131–140.
[12] B. Hernández, E. Peña, G. Pascual, M. Rodríguez, B. Calvo, M. Doblaré, J.M. Bellón, Mechanical and histological characterization of the abdominal muscle. a previous step to modelling hernia surgery, J Mech Behav Biomed Mater 4 (3) (2011) 392–404.
[13] D.A. Morrow, T.L. Haut Donahue, G.M. Odegard, K.R. Kaufman, Transversely isotropic tensile material properties of skeletal muscle tissue, J Mech Behav Biomed Mater 3 (1) (2010) 124–129.
[14] X. Nie, J.L. Cheng, W.W. Chen, T. Weerasooriya, Dynamic tensile response of porcine muscle, J Appl Mech 78 (2) (2011) 1–5.
[15] M. Takaza, K.M. Moerman, J. Gindre, G. Lyons, C.K. Simms, The anisotropic mechanical behaviour of passive skeletal muscle tissue subjected to large tensile strain, J Mech Behav Biomed Mater 17 (2013) 209–220.
[16] A.A.K. Yousefi, M.A. Nazari, P. Perrier, M.S. Panahi, Y. Payan, A new model of passive muscle tissue integrating collagen fibers: consequences for muscle behavior analysis, J Mech Behav Biomed Mater 88 (2018) 29–40.
[17] M. Böl, R. Kruse, A.E. Ehret, K. Leichsenring, T. Siebert, Compressive properties of passive skeletal muscle - the impact of precise sample geometry on parameter identification in inverse finite element analysis, J Biomech 45 (15) (2012) 2673–2679.
[18] J.H. McElhaney, Dynamic response of bone and muscle tissue, J Appl Physiol 21 (4) (1966) 1231–1236.
[19] R. Pietsch, B.B. Wheatley, T.L. Haut Donahue, R. Gilbrech, R. Prabhu, J. Liao, L.N. Williams, Anisotropic compressive properties of passive porcine muscle tissue, J Biomech Eng 136 (11) (2014) 1–8.
[20] B. Song, W. Chen, Y. Ge, T. Weerasooriya, Dynamic and quasi-static compressive response of porcine muscle, J Biomech 40 (13) (2007) 2999–3005.
[21] M. Takaza, K.M. Moerman, C.K. Simms, Passive skeletal muscle response to impact loading: experimental testing and inverse modelling, J Mech Behav Biomed Mater 27 (2013) 214–225.
[22] M. van Loocke, C.G. Lyons, C.K. Simms, A validated model of passive muscle in compression, J Biomech 39 (16) (2006) 2999–3009.
[23] M. van Loocke, C.G. Lyons, C.K. Simms, Viscoelastic properties of passive skeletal muscle in compression: stress-relaxation behaviour and constitutive modelling, J Biomech 41 (7) (2008) 1555–1566.
[24] M. van Loocke, C.K. Simms, C.G. Lyons, Viscoelastic properties of passive skeletal muscle in compression - cyclic behaviour, J Biomech 42 (8) (2009) 1038–1048.
[25] C. van Sligtenhorst, D.S. Cronin, G. Wayne Brodland, High strain rate compressive properties of bovine muscle tissue determined using a split hopkinson bar apparatus, J Biomech 39 (10) (2006) 1852–1858.
[26] P. Andrikakou, K. Vickraman, H. Arora, On the behaviour of lung tissue under tension and compression, Sci Rep 6 (2016) 1–10.
[27] S. Budday, G. Sommer, C. Birkl, C. Langkammer, J. Haybaeck, J. Kohnert, M. Bauer, F. Paulsen, P. Steinmann, E. Kuhl, G.A. Holzapfel, Mechanical characterization of human brain tissue, Acta Biomater 48 (2017) 319–340.
[28] C.Y. Huang, M.A. Soltz, M. Kopacz, C. van Mow, G.A. Ateshian, Experimental verification of the roles of intrinsic matrix viscoelasticity and tension-compression nonlinearity in the biphasic response of cartilage, J Biomech Eng 125 (1) (2003) 84–93.
[29] K.M. Myers, S. Socrate, A. Paskaleva, M. House, A study of the anisotropy and tension/compression behavior of human cervical tissue, J Biomech Eng 132 (2) (2010) 021003–1–021003–15.
[30] S. Xie, R.J. Wallace, A. Callanan, P. Pankaj, From tension to compression - asymmetric mechanical behaviour of trabecular bone's organic phase, Ann Biomed Eng 46 (6) (2018) 801–809.
[31] M. Takaza, G.M. Cooney, G. McManus, P. Stafford, C.K. Simms, Assessing the microstructural response to applied deformation in porcine passive skeletal muscle, J Mech Behav Biomed Mater 40 (2014) 115–126.
[32] M. Mohammadkhah, P. Murphy, C.K. Simms, The in vitro passive elastic response of chicken pectoralis muscle to applied tensile and compressive deformation, J Mech Behav Biomed Mater 62 (2016) 468–480.
[33] A. Listrat, B. Lebret, I. Louveau, T. Astruc, M. Bonnet, L. Lefaucheur, B. Picard, J. Bugeon, How muscle structure and composition influence meat and flesh quality, Sci World J (2016) 182746.
[34] S. Kohn, K. Leichsenring, R. Kuravi, A.E. Ehret, M. Böl, Direct measurement of the direction-dependent mechanical behaviour of skeletal muscle extracellular matrix, Acta Biomater 122 (2021) 249–262.
[35] M. Mohammadkhah, P. Murphy, C.K. Simms, Collagen fibril organization in chicken and porcine skeletal muscle perimysium under applied tension and compression, J Mech Behav Biomed Mater 77 (2018) 734–744.
[36] S.H.M. Brown, J.A. Carr, S.R. Ward, R.L. Lieber, Passive mechanical properties of rat abdominal wall muscles suggest an important role of the extracellular connective tissue matrix, J Orthop Res 30 (8) (2012) 1321–1326.
[37] R.L. Lieber, E. Runesson, F. Einarsson, J. Fridén, Inferior mechanical properties of spastic muscle bundles due to hypertrophic but compromised extracellular matrix material, Muscle & Nerve 28 (4) (2003) 464–471.
[38] M.A. Mathewson, H.G. Chambers, P.J. Girard, M. Tenenhaus, A.K. Schwartz, R.L. Lieber, Stiff muscle fibers in calf muscles of patients with cerebral palsy lead to high passive muscle stiffness, J Orthop Res 32 (12) (2014) 1667–1674.
[39] G.A. Meyer, R.L. Lieber, Elucidation of extracellular matrix mechanics from muscle fibers and fiber bundles, J Biomech 44 (4) (2011) 771–773.
[40] G. Mutungi, J. Trinick, K.W. Ranatunga, Resting tension characteristics in differentiating intact rat fast- and slow-twitch muscle fibers, J Appl Physiol 95 (6) (2003) 2241–2247.
[41] A. Tamura, S. Hayashi, T. Matsumoto, Effect of loading rate on viscoelastic properties and local mechanical heterogeneity of freshly isolated muscle fiber bundles subjected to uniaxial stretching, J Mech Med Biol 16 (6) (2016) 1–17.
[42] L.K. Wood, E. Kayupov, J.P. Gumucio, C.L. Mendias, D.R. Claflin, S.V. Brooks, Intrinsic stiffness of extracellular matrix increases with age in skeletal muscles of mice, J Appl Physiol 117 (4) (2014) 363–369.
[43] Y.N. Wu, Y. Ren, L.C. Tsai, F. Gao, L.Q. Zhang, In vivo simultaneous evaluations of sarcomere imaging and muscle fiber tension, J Biomech 49 (5) (2016) 797–801.
[44] S. Bensamoun, L. Stevens, M.J. Fleury, G. Bellon, F. Goubel, M.C. Ho Ba Tho, Macroscopic–microscopic characterization of the passive mechanical properties in rat soleus muscle, J Biomech 39 (3) (2006) 568–578.
[45] J. Fridén, R.L. Lieber, Spastic muscle cells are shorter and stiffer than normal cells, Muscle & Nerve 27 (2) (2003) 157–164.
[46] S.K. Gollapudi, D.C. Lin, Experimental determination of sarcomere force–length relationship in type-I human skeletal muscle fibers, J Biomech 42 (13) (2009) 2011–2016.

[47] M. Kammoun, P. Pouletaut, F. Canon, M. Subramaniam, J.R. Hawse, M. Vayssade, S.F. Bensamoun, Impact of TIEG1 deletion on the passive mechanical properties of fast and slow twitch skeletal muscles in female mice, PLoS ONE 11 (10) (2016) e0164566.
[48] G.A. Meyer, A.D. McCulloch, R.L. Lieber, A nonlinear model of passive muscle viscosity, J Biomech Eng 133 (9) (2011) 1–9.
[49] M.C. Olsson, M. Krüger, L.H. Meyer, L. Ahnlund, L. Gransberg, W.A. Linke, L. Larsson, Fibre type-specific increase in passive muscle tension in spinal cord-injured subjects with spasticity, J Physiol (Lond) 577 (2006) 339–352.
[50] M.L. Palmer, D.R. Claflin, J.A. Faulkner, A. Panchangam, Non-uniform distribution of strain during stretch of relaxed skeletal muscle fibers from rat soleus muscle, J Muscle Res Cell Motil 32 (1) (2011) 39–48.
[51] D.E. Rassier, E.J. Lee, W. Herzog, Modulation of passive force in single skeletal muscle fibres, Biol Lett 1 (3) (2005) 342–345.
[52] M.R. Rehorn, A.K. Schroer, S.S. Blemker, The passive properties of muscle fibers are velocity dependent, J Biomech 47 (3) (2014) 687–693.
[53] S.B. Shah, J. Davis, N. Weisleder, I. Kostavassili, A.D. McCulloch, E. Ralston, Y. Capetanaki, R.L. Lieber, Structural and functional roles of desmin in mouse skeletal muscle during passive deformation, Biophys J 86 (5) (2004) 2993–3008.
[54] T. Toursel, L. Stevens, H. Granzier, Y. Mounier, Passive tension of rat skeletal soleus muscle fibers - effects of unloading conditions, J Appl Physiol 92 (4) (2002) 1465–1472.
[55] M.L. Bartoo, W.A. Linke, G.H. Pollack, Basis of passive tension and stiffness in isolated rabbit myofibrils, Am J Physiol Cell Physiol 273 (1) (1997) C266–C276.
[56] A.L. Friedman, Y.E. Goldman, Mechanical characterization of skeletal muscle myofibrils, Biophys J 71 (5) (1996) 2774–2785.
[57] L.G. Prado, I. Makarenko, C. Andresen, M. Krüger, C.A. Opitz, W.A. Linke, Isoform diversity of giant proteins in relation to passive and active contractile properties of rabbit skeletal muscles, J Gen Physiol 126 (5) (2005) 461–480.
[58] K. Yasuda, T. Anazawa, S. Ishiwata, Microscopic analysis of the elastic properties of nebulin in skeletal myofibrils, Biophys J 68 (2) (1995) 598–608.
[59] M.C. Leake, D. Wilson, M. Gautel, R.M. Simmons, The elasticity of single titin molecules using a two-bead optical tweezers assay, Biophys J 87 (2) (2004) 1112–1135.
[60] W.A. Linke, M. Ivemeyer, P. Mundel, M.R. Stockmeier, B. Kolmerer, Nature of PEVK-titin elasticity in skeletal muscle, Proc Natl Acad Sci USA 95 (14) (1998) 8052.
[61] M. Böl, R. Iyer, J. Dittmann, M. Garcés-Schröder, A. Dietzel, Investigating the passive mechanical behaviour of skeletal muscle fibres - micromechanical experiments and bayesian hierarchical modelling, Acta Biomater 92 (2019) 277–289.
[62] M. Böl, R. Iyer, M. Garcés-Schröder, S. Kohn, A. Dietzel, Mechano-geometrical skeletal muscle fibre characterisation under cyclic and relaxation loading, J Mech Behav Biomed Mater 110 (2020) 104001.
[63] L.R. Smith, L. Gerace-Fowler, R.L. Lieber, Muscle extracellular matrix applies a transverse stress on fibers with axial strain, J Biomech 44 (8) (2011) 1618–1620.
[64] R. Kuravi, K. Leichsenring, M. Böl, A.E. Ehret, 3D finite element models from serial section histology of skeletal muscle tissue – the role of micro-architecture on mechanical behaviour, J Mech Behav Biomed Mater 113 (2021) 104109.
[65] R. Kuravi, K. Leichsenring, R. Trostorf, E. Morales-Orcajo, M. Böl, A.E. Ehret, Predicting muscle tissue response from calibrated component models and histology-based finite element models, J Mech Behav Biomed Mater 117 (2021) 104375.
[66] T. Ahamed, M.B. Rubin, B.A. Trimmer, L. Dorfmann, Time-dependent behavior of passive skeletal muscle, Continuum Mech Thermodyn 28 (1) (2016) 561–577.
[67] M. Böl, K. Leichsenring, C. Weichert, M. Sturmat, P. Schenk, R. Blickhan, T. Siebert, Three-dimensional surface geometries of the rabbit soleus muscle during contraction - input for biomechanical modelling and its validation, Biomech Model Mechanobiol 12 (6) (2013) 1205–1220.
[68] M. Böl, K. Leichsenring, M. Ernst, C. Wick, R. Blickhan, T. Siebert, Novel microstructural findings in m. plantaris and their impact during active and passive loading at the macro level, J Mech Behav Biomed Mater 51 (2015) 25–39.
[69] A.C. Abraham, K.R. Kaufman, T.L. Haut Donahue, Phenomenological consequences of sectioning and bathing on passive muscle mechanics of the new zealand white rabbit tibialis anterior, J Mech Behav Biomed Mater 17 (2013) 290–295.
[70] L.L. Gras, D. Mitton, P. Viot, S. Laporte, Viscoelastic properties of the human sternocleidomastoideus muscle of aged women in relaxation, J Mech Behav Biomed Mater 27 (2013) 77–83.
[71] L.L. Gras, S. Laporte, P. Viot, D. Mitton, Experimental characterization of post rigor mortis human muscle subjected to small tensile strains and application of a simple hyper-viscoelastic model, Proc Inst Mech Eng H: J Eng Med 228 (10) (2014) 1059–1068.
[72] N. Jalal, M. Zidi, Effect of cryopreservation at -80°c on visco-hyperelastic properties of skeletal muscle tissue, J Mech Behav Biomed Mater 77 (2018) 572–577.
[73] D. Morrow, T. Donahue, G. Odegard, K. Kaufman, Tensile material properties of skeletal muscle tissue in longitudinal and transverse directions, Proceedings of the ASME Summer Bioengineering Conference, SBC2008 (2008).
[74] A.S. Nagle, M.A. Barker, S.D. Kleeman, B. Haridas, T. Douglas Mast, Passive biomechanical properties of human cadaveric levator ani muscle at low strains, J Biomech 47 (2) (2014) 583–586.
[75] B.B. Wheatley, G.M. Odegard, K.R. Kaufman, T.L.H. Donahue, How does tissue preparation affect skeletal muscle transverse isotropy? J Biomech 49 (13) (2016) 3056–3060.
[76] L. Yoo, H. Kim, V. Gupta, J.L. Demer, Quasilinear viscoelastic behavior of bovine extraocular muscle tissue, Investigative Ophthalmology & Visual Science 50 (8) (2009) 3721–3728.
[77] A. Chawla, S. Mukherjee, B. Karthikeyan, Characterization of human passive muscles for impact loads using genetic algorithm and inverse finite element methods, Biomech Model Mechanobiol 8 (1) (2009) 67–76.
[78] T.J. Noonan, T.M. Best, A.V. Seaber, W.E. Garrett, Thermal effects on skeletal muscle tensile behavior, Am J Sports Med 21 (4) (1993) 517–522.
[79] M. Böl, A.E. Ehret, K. Leichsenring, M. Ernst, Tissue-scale anisotropy and compressibility of tendon in semi-confined compression tests, J Biomech 48 (6) (2015) 1092–1098.
[80] M.A. Soltz, G.A. Ateshian, A conewise linear elasticity mixture model for the analysis of tension-compression nonlinearity in articular cartilage, J Biomech Eng 122 (6) (2000) 576–586.
[81] K.M. Myers, C.P. Hendon, Y. Gan, W. Yao, K. Yoshida, M. Fernandez, J. Vink, R.J. Wapner, A continuous fiber distribution material model for human cervical tissue, J Biomech 48 (9) (2015) 1533–1540.
[82] J. Gindre, M. Takaza, K.M. Moerman, C.K. Simms, A structural model of passive skeletal muscle shows two reinforcement processes in resisting deformation, J Mech Behav Biomed Mater 22 (2013) 84–94.
[83] F.J. Carter, T.G. Frank, P.J. Davies, D. McLean, A. Cuschieri, Measurements and modelling of the compliance of human and porcine organs, Med Image Anal 5 (4) (2001) 231–236.
[84] C. Chui, E. Kobayashi, X. Chen, T. Hisada, I. Sakuma, Combined compression and elongation experiments and non-linear modelling of liver tissue for surgical simulation, Med Biol Eng Comput 42 (6) (2004) 787–798.
[85] P.J. Davies, F.J. Carter, A. Cuschieri, Mathematical modelling for keyhole surgery simulations: a biomechanical model for spleen tissue, IMA J Appl Math 67 (1) (2002) 41–67.
[86] V. Libertiaux, F. Pascon, S. Cescotto, Experimental verification of brain tissue incompressibility using digital image correlation, J Mech Behav Biomed Mater 4 (7) (2011) 1177–1185.
[87] K. Miller, K. Chinzei, G. Orssengo, P. Bednarz, Mechanical properties of brain tissue in-vivo: experiment and computer simulation, J Biomech 33 (11) (2000) 1369–1376.
[88] A. Nava, E. Mazza, M. Furrer, P. Villiger, W.H. Reinhart, In vivo mechanical characterization of human liver, Med Image Anal 12 (2) (2008) 203–216.
[89] N.H. Nguyen, M.T. Duong, T.N. Tran, P.T. Pham, O. Grottke, R. Tolba, M. Staat, Influence of a freeze–thaw cycle on the stress–stretch curves of tissues of porcine abdominal organs, J Biomech 45 (14) (2012) 2382–2386.
[90] B. Rashid, M. Destrade, M.D. Gilchrist, Mechanical characterization of brain tissue in simple shear at dynamic strain rates, J Mech Behav Biomed Mater 28 (2013) 71–85.
[91] E. Roan, K. Vemaganti, The nonlinear material properties of liver tissue determined from no-slip uniaxial compression experiments, J Biomech Eng 129 (3) (2006) 450–456.
[92] A. Samani, D. Plewes, A method to measure the hyperelastic parameters ofex vivobreast tissue samples, Phys Med Biol 49 (18) (2004) 4395–4405.
[93] R.W. Ogden, Non-linear elastic deformations, Dover Publications, 1997.
[94] A.E. Ehret, K. Bircher, A. Stracuzzi, V. Marina, M. Zündel, E. Mazza, Inverse poroelasticity as a fundamental mechanism in biomechanics and mechanobiology, Nat Commun 8 (1) (2017) 1002.
[95] R.H. Baughman, S. Stafström, C. Changxing, S.O. Dantas, Materials with negative compressibilities in one or more dimensions, Science 279 (5356) (1998) 1522–1524.
[96] A. Stracuzzi, E. Mazza, A.E. Ehret, Chemomechanical models for soft tissues based on the reconciliation of porous media and swelling polymer theories, J Appl Math Mech 98 (12) (2018) 2135–2154.
[97] C.K. Simms, M. van Loocke, C.G. Lyons, Skeletal muscle in compression: modeling approaches for the passive muscle bulk, Int J Multiscale Comput Eng 10 (2) (2012).
[98] S.W. Chi, J. Hodgson, J.S. Chen, V. Reggie Edgerton, D.D. Shin, R.A. Roiz, S. Sinha, Finite element modeling reveals complex strain mechanics in the aponeuroses of contracting skeletal muscle, J Biomech 43 (7) (2010) 1243–1250.
[99] O. Röhrle, A.J. Pullan, Three-dimensional finite element modelling of muscle forces during mastication, J Biomech 40 (15) (2007) 3363–3372.
[100] B. Sharafi, S.S. Blemker, A micromechanical model of skeletal muscle to explore the effects of fiber and fascicle geometry, J Biomech 43 (16) (2010) 3207–3213.
[101] L.A. Spyrou, A computational multiscale modeling framework for investigating the mechanical properties of meat, Food Structure 26 (2020) 100161.
[102] L.A. Spyrou, S. Brisard, K. Danas, Multiscale modeling of skeletal muscle tissues based on analytical and numerical homogenization, J Mech Behav Biomed Mater 92 (2019) 97–117.
[103] K.M. Virgilio, K.S. Martin, S.M. Peirce, S.S. Blemker, Multiscale models of skeletal muscle reveal the complex effects of muscular dystrophy on tissue mechanics and damage susceptibility, Interface Focus 5 (2) (2015) 20140080.